Quantitative estimation for the impact of mining activities on vegetation phenology and identifying its controlling factors from Sentinel-2 time series

Xiaofei Sun, Linguo Yuan, Meng Liu, Shuneng Liang, Dongfeng Li, Liyang Liu

International Journal of Applied Earth Observations and Geoinformation 111 (2022) 102814

Contents lists available at ScienceDirect

International Journal of Applied Earth Observations and Geoinformation

journal homepage: www.elsevier.com/locate/jag

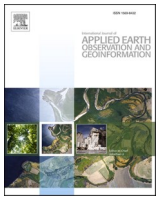

Quantitative estimation for the impact of mining activities on vegetation phenology and identifying its controlling factors from Sentinel-2 time series

Xiaofei Sun [a,c], Linguo Yuan [a,*], Meng Liu [b,*], Shuneng Liang [d], Dongfeng Li [c], Liyang Liu [e,*]

[a] Faculty of Geosciences and Environmental Engineering, Southwest Jiaotong University, Chengdu 611756, China
[b] Key Laboratory of Agricultural Remote Sensing, Ministry of Agriculture and Rural Affairs/Institute of Agricultural Resources and Regional Planning, Chinese Academy of Agricultural Sciences, Beijing 100081, China
[c] Department of Geography, National University of Singapore, Kent Ridge 117570, Singapore
[d] Land Satellite Remote Sensing Application Center, Ministry of Natural Resources of China, Beijing 100048, China
[e] Laboratoire des Sciences du Climat et de l'Environnement, IPSL, CEA-CNRS-UVSQ, Université Paris-Saclay, 91191 Gif sur Yvette France

ARTICLE INFO

Keywords:
Remote sensing
Sentinel-2 time series
Vegetation phenology
Mining area
Pareto principle

ABSTRACT

Quantitative assessment of the negative environmental effects of mining is vital for the eco-environmental restoration and management of mining areas. However, it remains unclear about the spatial dimension of the influence on the environment that comes from mining. Here, we constructed a new method to quantify the vegetation impact of mining activity using Sentinel-2 time series and Pareto principle, and applied it to the Liaoning Nanfen iron mining area (LNMA), the Inner Mongolia Sanheming iron mining area (IMMA), and the Sichuan Hongge iron mining area (SCMA) in China. Based on the unequal relationship of 80% of the consequences determined by 20% of the causes, the influence of mining activities on vegetation was quantified by the maximum phenological difference, the decay rate, the asymptotic value of exponential trend and the distance from the mine. Results showed that the impact of mining activities on vegetation phenology decayed exponentially along with the increase of the distance to the mines. The influence distance of mining activities on vegetation were 1566.95 m, 1959.67 m, and 1809.61 m for LNMA, IMMA and SCMA, respectively. Compared to areas 5 km away from the mining activity, the start of the growing season for vegetation surrounding the mining activity was delayed by 1.1 ± 0.4 days, 6.1 ± 1.9 days, and 1.5 ± 0.7 days for LNMA, IMMA and SCMA, respectively, while the length of the growing season was successively shortened by 1.0 ± 0.6 days, 5.4 ± 2.5 days, and 5.1 ± 3.9 days, respectively. Our investigation found that the dust pollution, decreases in groundwater levels, and waterborne pollution were the main factors that directly caused phenological changes around the mining area, and the distance and degree of their impact on phenology were closely related to drought and topography. This finding could provide a reference for the environmental restoration and management of mining areas and help to add insights on the assessment for the long-term impacts of mining activities on vegetation.

1. Introduction

The mining industry is a significant contributor to the national economy (Litvinenko, 2020) and plays a serious and strategic role in its economic development (Firozjaei et al., 2021). Although the mining industry significantly impacts social welfare (Sonderegger et al., 2020), it has also caused long-term negative effects on the eco-environment around mining areas. Intensive mining activities have often led to the degradation of land as well as deforestation, topographic and hydrological changes, soil erosion, and environmental pollution, severely damaging the health of countless organisms (Odell et al., 2018; Tost et al., 2018). If the impacts of mining activities on the environment do not arouse enough attention by the authorities, it will impose a double cost for the ecological restoration in mining areas (Maryati et al., 2012). Thus, attaching great importance to the impact of mining activities on the surrounding environment is necessary for mine ecological restoration, planning, and pattern optimization.

The advancement of satellite-to-earth observation technology provides a systematic, fast, and excellent configuration for processing large and complex spatial data. Therefore, many researchers have demonstrated the importance of satellite-to-earth observation technology in studying the impact of the mining industry on the eco-environment.

* Corresponding authors.
E-mail addresses: lgyuan@swjtu.edu.cn (L. Yuan), liumeng01@caas.cn (M. Liu), liuliyang18@mails.ucas.ac.cn (L. Liu).

https://doi.org/10.1016/j.jag.2022.102814
Received 24 February 2022; Received in revised form 15 April 2022; Accepted 7 May 2022
Available online 2 June 2022

First, the size and location distribution of the mines were determined using satellite images. Chaussard and Kerosky (2016)Chaussard et al. (2016) provided a reliable, safe, cost-effective, and objective way to investigate black sand mining and its impacts via a systematic analysis of remote sensing (RS) data. Forkuor et al. (2020) and Gallwey et al. (2020) believed that RS data could be used to monitor illegal mining sites and characterize the direct impact of mining on the environment. Second, RS and geographic information systems (GIS) were used as analytical tools to assess the impact of mining activities on the eco-environment. Shao et al. (2021) and He et al. (2017) indicated that mining intensity and eco-environment restoration were the main factors determining the changes in the environment of the mines area. Rudke et al. (2020) analyzed the concentration of mining projects in the southwestern Amazon. They used RS and GIS to create a mining pressure index (MPI) to evaluate the impact of mining activities on environmental protection areas. Third, explore one or more impacts of mining activities on water, land and society. Castellazzi et al. (2018) used a combination of GRACE and InSAR data to map groundwater in a mining area. Yu et al. (2018) used multiple RS datasets to investigate the impact of mining on land cover globally from the 1980 s to 2013. McDonald et al. (2012) analyzed the social and economic impact of mine closures from a spatial perspective. Although the above studies have analyzed the impact of mining activities on the environment using RS and GIS technology, the spatial dimension of mining impacts on the surrounding environment remains unclear.

Vegetation is one of the comprehensive indicators for assessing environmental changes (Parmesan et al., 2003). Numerous sources of disturbance (geological hazards, groundwater decline, environmental pollution) caused by mining activities often bury entire plant communities and damage their roots, leading to their degradation (Mi et al., 2019). Therefore, quantifying the spatial dimension of the mining impacts on the eco-environment by determining the mining impact on vegetation is feasible and challenging. Long-term serial phenological observation is an effective method by which to distinguish changes in vegetation caused by natural and human activities as it can reveal trends in the changes that could be caused by external forces (Verbesselt et al., 2010). In recent years, most existing land surface phenology (LSP) studies have used data from coarse spatial resolution instruments (e.g., MODIS and AVHRR) (Kandasamy and Fernandes, 2015; Adole et al., 2018; Zhang et al., 2020). Data from such coarse spatial resolution instruments have generally become easier to process and are easily available, making LSP algorithms, products, and applications have rapidly matured and expanded. However, for many applied studies (e.g., microclimatic effects, urban heat islands, and land use), information is required at finer spatial resolutions (Bolton et al., 2020; Gao et al., 2021). Recently, with the successful launch of the Sentinel-2 (S2) satellite, optical images with a revisit period of 5 days and a spatial resolution of 10 m have been made available; these images largely resolve constraints and help improve the phenological observation of vegetation around the mining area. The main objectives of this study were based on S2 image to investigate (1) the degree and distance of the impact of mining activities on phenology, (2) the main factors in the impact of different mining areas on phenology, and (3) factors controlling of the impact of mining activities on phenology.

2. Study area and materials

2.1. Study area

Three typical iron mining areas in China, namely, Liaoning Nanfen iron mining area (41° 06′ 14″ N, 123° 36′ 10″ E, LNMA), Inner Mongolia Sanheming iron mining area (41° 21′ 25″ N, 110° 59′ 59″ E, IMMA), and Sichuan Hongge iron mining area (26° 39′ 21″ N, 101° 59′ 49″ E, SCMA) were selected as study areas (Fig. 1). These mining areas were selected

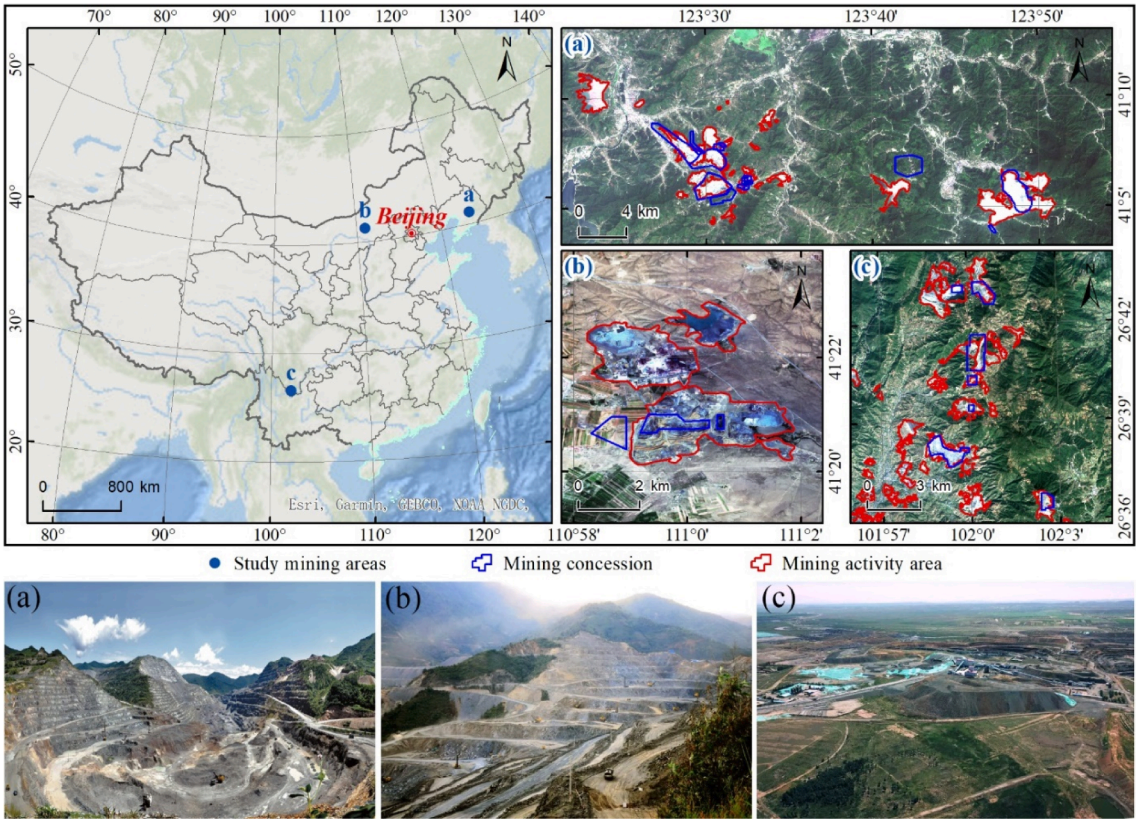

Fig. 1. Geographical location of the case and the distribution of its mining activities. (a) Liaoning Nanfen iron mining area; (b) Inner Mongolia Sanheming iron mining area; (c) Sichuan Hongge iron mining area.

because (1) they were large in scale and had outstanding eco-environmental problems (Dai et al., 2021); (2) besides mining activities, there were few other human activities around the mining areas; and (3) there were enough cloud-free S2 images available to investigate the impact of mining activities on vegetation phenology. Additionally, these mining areas had different climate types. LNMA had a temperate monsoon climate, IMMA had a dry inland climate, and SCMA had a subtropical monsoon climate. Thus, comparing these three mining areas enabled us to understand better the impact of mining activities on the surrounding vegetation phenology in different environments.

2.2. Materials

2.2.1. Dataset

We compared data availability and cloud cover ratios of all S2 (L1C, Level-1C) images from the USGS (https://earthexplorer.usgs.gov) during the growth cycle of vegetation surrounding the three mining areas. According to the Sentinel-CLD band classification standard (Main-Knorn et al. 2015), a total of 229 S2 images from 2018 to 2020 with low cloud probability were selected to obtain dense time series data, from which the vegetation phenological metrics for the study areas were obtained. Specifically, LNMA, IMMA and SCMA had 81 images, 73 images, and 75 images, respectively, which could provided adequately clear observations to capture the growth cycle of vegetation around the mining area. Before using these images, L2A (Level-2A) bottom of the atmosphere reflectance products was obtained by performing atmospheric correction of the L1C images with Sen2Cor software (Sola et al., 2018). Additionally, the digital elevation model with 30 m spatial resolution was obtained from NASA (Earthdata Search, https://earthdata.nasa.gov/), and the meteorological data was collected from the National Meteorological Information Centre (https://data.cma.cn/en). These materials were used to analyze the relationship between vegetation phenology of surrounding the mining area and its climatic background and topography.

2.2.2. Image preprocessing

Preprocessing the S2 (L1C) image consisted of three steps. The first step was screening cloudy and shadow pixels. The accuracy of cloud and shadow masks were critical for minimizing errors in processing time-series data from satellites (Misra et al., 2020). Therefore, the newly released Fmask 4.0 (Qiu et al., 2019) was applied to the cloud and shadow pixel detection of S2 images. Although Sen2Cor can detect cloud and shadow coverage, it easily misclassifies urban areas and bright pixels as clouds, limiting its scene classification (Baetens et al., 2019). The second step was the surface water mask. The normalized difference water index and the threshold method were used to identify and eliminate pixels dominated by surface water. The third step involved the calculation of the normalized difference vegetation index (NDVI). As NDVI has a strong correlation with vegetation greenness and biomass, it is commonly used in vegetation phenology research (Hmimina et al., 2013; Norris and Walker, 2020). Here, the near-infrared (NIR) and red bands of the S2 images were used to calculate NDVI:

$$NDVI = \frac{\rho_{NIR} - \rho_{red}}{\rho_{NIR} + \rho_{red}} \quad (1)$$

where ρ_{red} and ρ_{NIR} are band 4 and band 8 of the S2 image, respectively.

In order to distinguish between vegetation and other land use types, the support vector machine (SVM) classifier was used to divide the land cover of the study area into six categories (i.e., forestland, grassland, farmland, waterbody, construction land, and other land covers) (Fig. 2). The accuracy of the classification results was evaluated using high-resolution images from Google Earth; moreover, Kappa statistics of all classification results were greater than 0.85. For complete details on using SVM classifiers to classify S2 images, please refer to the work of Thanh and Kappas (2018).

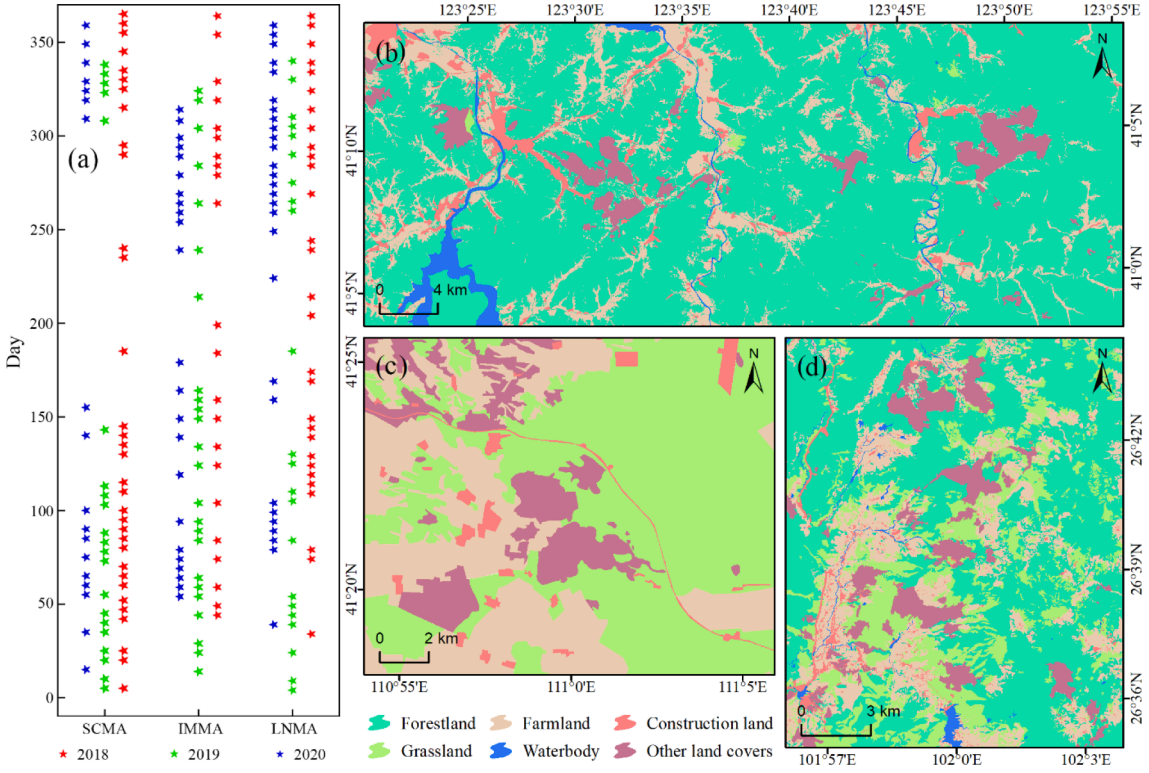

Fig. 2. (a) Selection of Sentinel-2 L1C images. The land use type distribution of (b) Liaoning Nanfen iron mining area; (c) Inner Mongolia Sanheming iron mining area; (d) Sichuan Hongge iron mining area.

3. Methodology

3.1. Data smoothing

The initially generated NDVI time series contained various noises. Thus, it was necessary to convert the noisy NDVI time series into a smooth time series before identifying the vegetation phenological metrics to minimize residual noise. Existing research has fitted several models to smooth NDVI time series from different data sources to extract phenological metrics. However, fine-tuning the model parameters and differences between the models affects the extraction of vegetation phenological metrics from the smoothed NDVI time series data (Atkinson et al., 2012). At present, choosing the optimal method for smoothing time series is very difficult. Furthermore, when choosing the most appropriate method, biogeographical characteristics of the study area, targeted phenological metrics, potential noise sources in the NDVI data, and general shape of NDVI time series curves should be considered (Hird and Mcdermid, 2009). Therefore, this study selected four commonly used models: Double Logistic filter (DL), Savitzky-Golay filter (S-G), Asymmetric Gaussian filter (AG), and Harmonic Analysis of Time Series (HANTS) to smooth the initial NDVI time series. As noise and gaps in the initial data can negatively influence the realism of the smoothed NDVI, multi-year (2018–2020) imagery from S2 was merged within a single phenological time series to eliminate the impact of both sources of uncertainty (Melaas et al., 2016).

3.1.1. Harmonic analysis of time series

HANTS decomposes the time-spectrum data into many sines and cosine curves of different frequencies, selects the curves that can represent the time series and superimposes them to reconstruct the time series data (Padhee and Dutta, 2019). In essence, the harmonic fit is a linear regression between an independent variable and a dependent variable. The basic formula is expressed as:

$$R_N^{i,j} = a_0 + \sum_{n=1}^{N} a_n cos\left(2\pi f_n t^{i,j}\right) + b_n sin\left(2\pi f_n t^{i,j}\right) \quad (2)$$

$$O_N^{i,j} = R_N^{i,j} + \beta^{i,j} \quad (3)$$

where R_N represents the smoothed NDVI time series; O_N represents the initial NDVI time series; β represent the error series; f represents frequency; n and N represent the number and maximum number of harmonic components related to f, respectively; (i, j) represents the position of the pixel; t represents the time corresponding to the NDVI time series; a_0 represents the baseline constant; a_n represents the coefficient of the cosine component with f_n; b_n represents the coefficient of the sine component with f_n.

3.1.2. Savitzky-Golay

The S-G is based on the average trend of the NDVI time series curve to determine the appropriate filter parameters and use polynomials to achieve the least-squares fitting in the filter window (Chen et al., 2004). The basic formula is expressed as:

$$RY_j = \sum_{i=-k}^{i=k} W_i Y_{j+1}/N \quad (4)$$

where RY_j represents the smoothed NDVI time series; Y represents the initial NDVI time series. W_i represents the filter parameters of the *i-th* NDVI value in the filter window. N represents the number of convoluting integers, and k is a parameter that determines the filter window size; j represents the j-th data in the NDVI time series.

3.1.3. Asymmetric Gaussian

AG fits local nonlinear functions at the local minimum and maximum intervals, and then the NDVI time series reconstruction is realized by smoothly connecting the fitting curves (Jönsson and Eklundh, 2002). The basic formula for AG is expressed as:

$$G(t) = \begin{cases} exp\left[-\left(\frac{t-p_1}{p_2}\right)^{p_3}\right], t > p_1 \\ exp\left[-\left(\frac{p_1-t}{p_4}\right)^{p_5}\right], t < p_1 \end{cases} \quad (5)$$

where $G(t)$ represents the smoothed NDVI value at time t, p_1 represents the minimum (or maximum) position (in time), p_2 and p_3 represent the flatness and width of the right half function, and p_4 and p_5 represent the flatness and width of the left half function, respectively.

3.1.4. Double Logistic

DL is a new time series analysis method proposed by Efron B in 1986 (Efron, 1986). This method is applied to the remote sensing investigating of vegetation phenology and can effectively estimate various parameters related to vegetation phenology, such as the start of the growing season (SOS), the end of the growing season (EOS), and the length of the growing season (LOS) (Beck et al., 2006). Compared to other approaches, this model captures the vegetation green-up and senescence phases well, and the physical meaning of the parameters is related to vegetation growth and senescence (Li et al., 2019). The basic formula for DL is expressed as:

$$X(t) = \frac{1}{1+\exp\left(\frac{d_1-t}{d_2}\right)} - \frac{1}{1+\exp\left(\frac{d_3-t}{d_4}\right)} \quad (6)$$

where $X(t)$ represents the smoothed NDVI value at time t; d_1- d_4 are position and shape parameters; d_1 and d_3 are the positions of the left and right inflection points, respectively. d_2 and d_4 determine the change rate of the left and right inflection points, respectively.

The HANTS approach was tested with its interactive data language (IDL) implementations, and the parameter settings in the fitting process were as: (1) the number of frequencies was 3; (2) suppression flag was low; (3) the high threshold was 1, and the low threshold was 0 in the invalid data rejection threshold setting; (4) fit error tolerance was 0.05; (5) degree of over-determinedness was 20; and (6) damping factor was 0.5. The S-G, AG and DL approaches were carried out through the TIMESAT package (Jönsson and Eklundh, 2004).

3.2. Extraction of vegetation phenological metrics

This study focused on three phenological metrics, namely SOS, EOS, and LOS. They were extracted using smoothed NDVI time series. To date, many methods have been proposed to extract phenological metrics; these include the threshold method (Zhang and Goldberg, 2011), moving average method (Ivits et al., 2012), and largest derivative (Xin et al., 2020). Among these, the threshold method is the simplest for extracting phenological metrics and is also the most commonly used. Usually, there are two types of threshold methods: (1) a fixed threshold that arbitrarily determines a fixed and single index value as SOS or EOS and (2) a dynamic threshold, which is generally based on a metric calculated from the smoothed time series data, such as the long-term median, mean and ratio of the time series data record. As the NDVI value in the mining activity area is much lower than that of the surrounding areas, it is difficult to accurately find the thresholds for determining the SOS and EOS dates. Therefore, by referring to existing studies (Buyantuyev and Wu, 2012; Zhou et al., 2016), this study defined SOS and EOS as 20% of the seasonal amplitude measured from the lowest level on the left and right, respectively (Fig. 3).

3.3. A method for quantifying the impact of mining activities on phenology

Generally, the negative impact of mining activities on the environment often decreases as the distance from the mine increases. Buffer

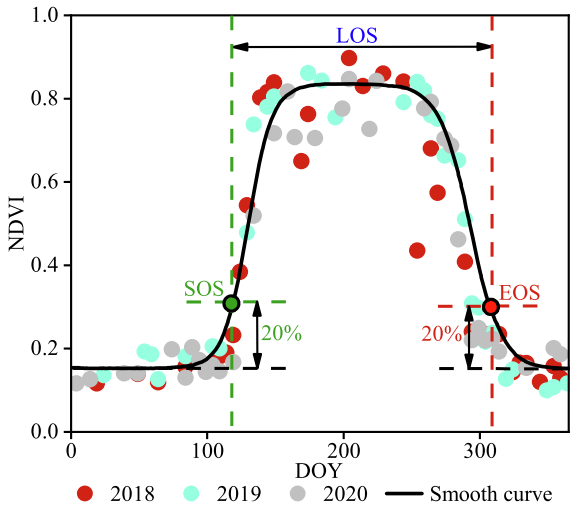

Fig. 3. Schematic diagram of extract phenological metrics. The selected pixels are in the Liaoning Nanfen iron mining area (41° 06′ 35.211″ N, 123° 51′ 05.094″ E). DOY, day of the year.

analysis is an effective method for identifying the impact range of mining activities on the surrounding environment. According to Wu et al. (2020), the theoretical reference range for the impact of mining on the surrounding environment is 5000 m. Therefore, mining activity vectors were used to create 25 buffer zones with a distance of 200 m. In order to quantify the impact of mining activities and eliminate the effects of climate on vegetation as much as possible, the average phenology outside the buffer zone was chosen as the reference. Next, the impact of mining activities on phenology was discussed at the buffer scale for three mining areas. The average of the phenological metrics in each buffer zone was counted, and the phenology difference between the buffer zone and the reference zone were calculated using Eq. (7). Subsequently, the phenological difference at different distances of the buffer zone was applied for quantifying the impact of mining activities on vegetation. Finally, the spatial distribution of the impact of mining activities on the surrounding vegetation was analyzed according to the calculated influence distance and the degree of influence. In addition, cropland was excluded because human activities controlled the planting and harvesting of crops.

$$\Delta P = P_m - P_r \tag{7}$$

Where ΔP is the phenological difference in the buffer zone, P_m is the mean of the phenological metrics in the buffer zone, and P_r is the reference phenology.

This study analyzed the trends in phenological differences from the mine to the reference areas, and the reference similar study (Zhou et al., 2015) found that the phenological differences from the mine to the reference area changed exponentially with distance (Fig. 4). Given that there was no inflection point in the fitted curve, it was difficult to quantify the spatial distance of the impact of mining activities. To this end, the Pareto principle (Espada, 2018) was introduced to quantify the influence distance of mining activities on vegetation. This principle believes that there is an unequal relationship between outputs and inputs, and 80% of the consequences are caused by 20% of the causes (Rohith and Kumar, 2020). In Fig. 4, "Part A" contains 80% of the information on the impact of mining activities on vegetation phenology, while "Part B" contains less information that can be omitted. Therefore, the distance corresponding to the dividing point between "Part A" and "Part B" is defined as the influence distance of mining activities. Based on the fitting equation and Pareto principle, the model to quantify the spatial distance of the impact of mining activities on vegetation can be expressed as:

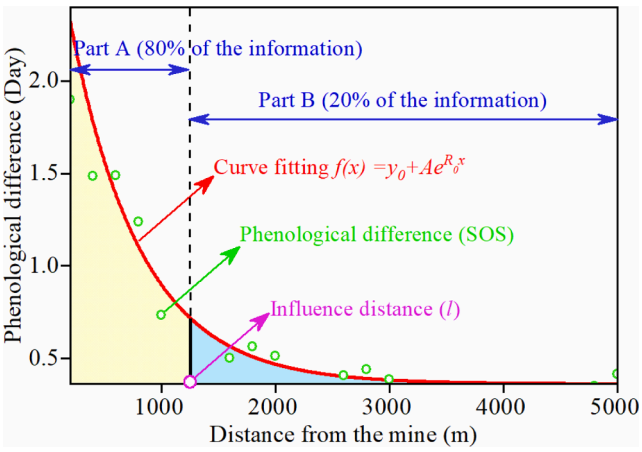

Fig. 4. Conceptual model to quantify the influence distance of mining activities.

$$\int_0^l f(x)dx = \frac{4}{5}\left(\frac{Ae^{nR_0} - A}{R_0} + ny_0\right) \tag{8}$$

The fitting equation is $f(x) = y_0 + Ae^{R_0 x}$, where A represents the maximum phenological difference, R_0 represents the decay rate, and y_0 represents the asymptotic value of exponential trend; n represents the distance from the mine to the reference area; l represents the influence distance.

4. Results

4.1. Vegetation phenology in the mining area

Fig. 5 shows the spatial distribution of the phenological metrics obtained by different smoothing methods. The results passed the T-test at the 95% confidence level (Press et al., 1992), and outliers were excluded. The spatial patterns of the vegetation phenology were similar in each mining area; that is, the SOS was delayed compared to areas away from the mining area; the LOS was shorter than the area away from the mining area, especially in IMMA (Fig. 5b). The impact of mining activities on EOS was small, and there was no obvious difference in the spatial distribution. Fig. 6 shows the median of the vegetation phenological metrics derived from the different models, which indicates that the results depend on the choice of the model. For example, HANTS first reached SOS, and the SOS obtained by SG, AG, and DL varied with the mining area. In general, the mean SOS (mean of the median) of LNMA, IMMA, and SCMA were DOY 109, DOY 176, and DOY 155, respectively. Moreover, the EOS in the three mining areas were similar and were reached in the following order: DL, AG, SG, and HANTS; The mean EOS of LNMA, IMMA, and SCMA were DOY 307, DOY 276, and DOY 364, respectively. With respect to LOS, SCMA had the longest LOS duration (approximately 214 days), followed by LNMA (192 days); IMMA had the shortest duration (96 days). Overall, the LOS in low latitudinal regions (SCMA) was generally longer than that in high latitudinal regions (LNMA and IMMA), and this phenomenon was also found by Zhang et al. (2007).

4.2. Changes of phenological metrics in the mining area

Fig. 7 shows the mean of phenological metrics and the fitted curve for every 200 m buffer zone. Clearly, the ΔSOS, ΔEOS, and ΔLOS obtained by the four smoothing methods showed an exponential change with an increase in the distance from the mining area, and the changing trend was consistent. Changes in ΔSOS and ΔLOS were the most obvious, while the change in ΔEOS was relatively weak. Based on the Pareto principle, the influence distance of mining activities on

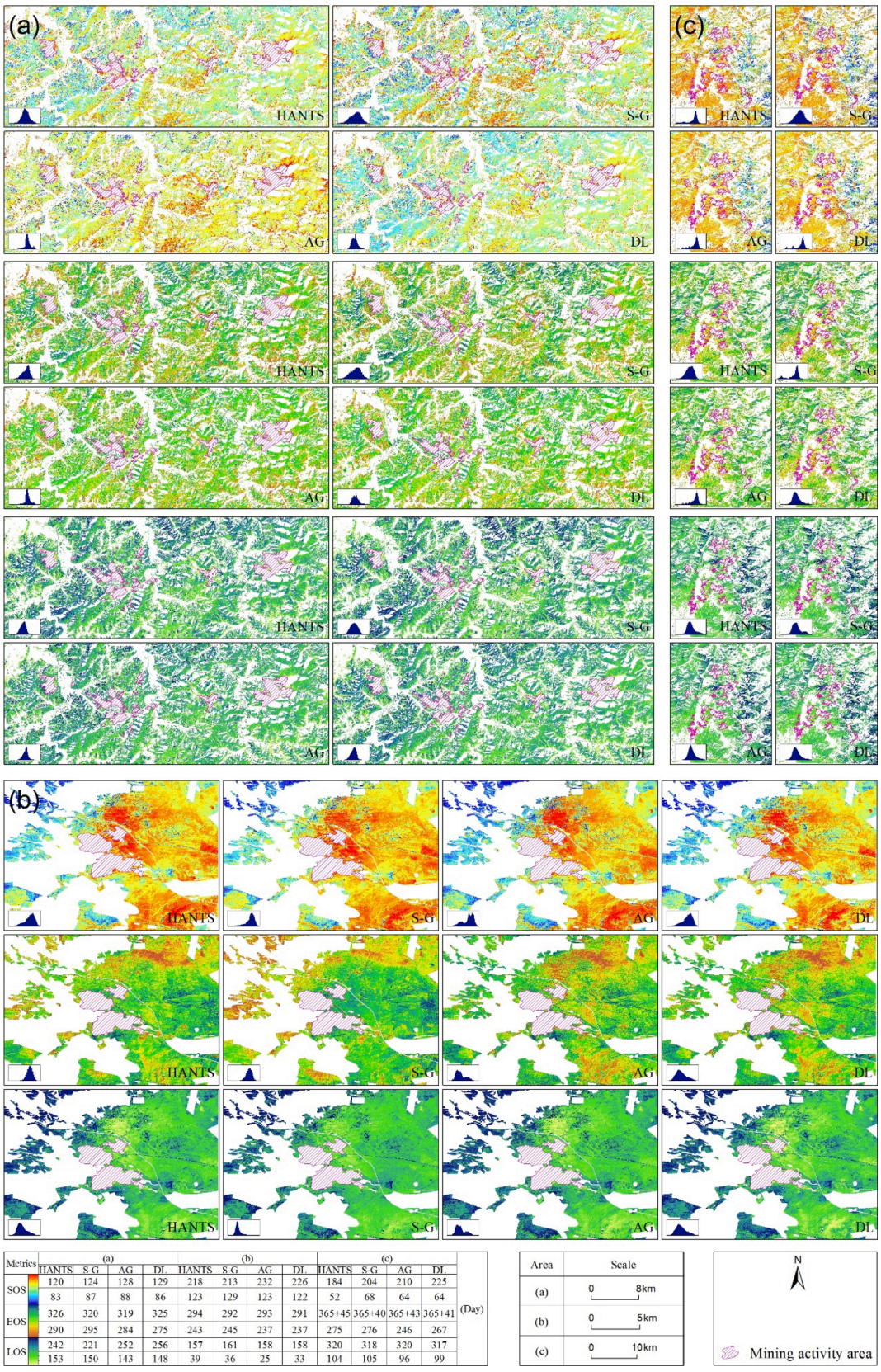

Metrics	(a) HANTS	(a) S-G	(a) AG	(a) DL	(b) HANTS	(b) S-G	(b) AG	(b) DL	(c) HANTS	(c) S-G	(c) AG	(c) DL
SOS	120	124	128	129	218	213	232	226	184	204	210	225
	83	87	88	86	123	129	123	122	52	68	64	64
EOS	326	320	319	325	294	292	293	291	365|45	365|40	365|43	365|41
	290	295	284	275	243	245	237	237	275	276	246	267
LOS	242	221	252	256	157	161	158	158	320	318	320	317
	153	150	143	148	39	36	25	33	104	105	96	99

(Day)

Area	Scale
(a)	0 8km
(b)	0 5km
(c)	0 10km

Fig. 5. Spatial distribution of phenological metrics in the mining areas. (a) Liaoning Nanfen iron mining area; (b) Inner Mongolia Sanheming iron mining area; (c) Sichuan Hongge iron mining area.

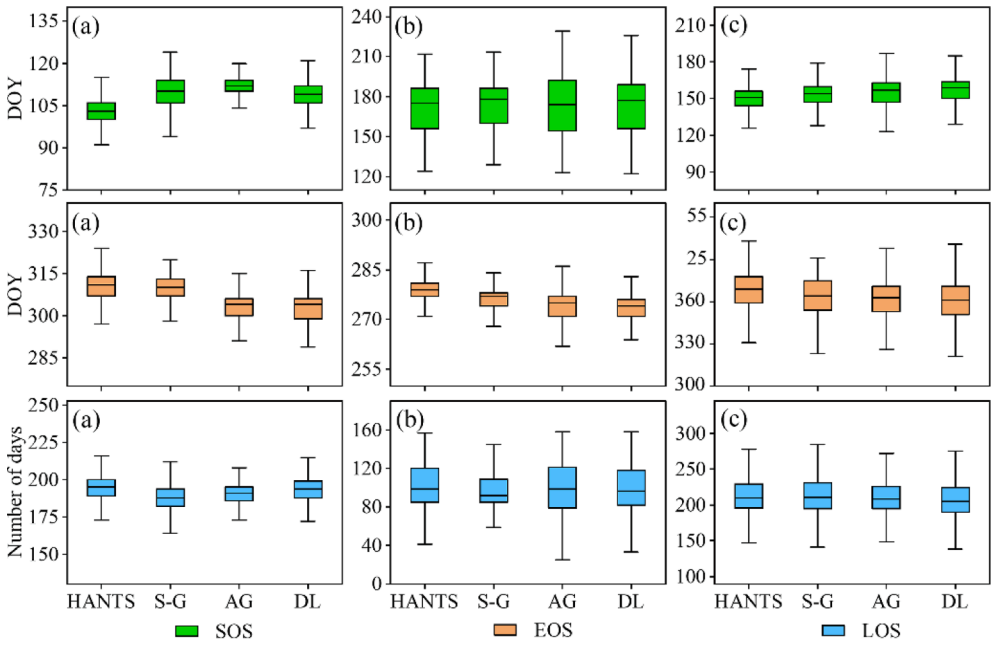

Fig. 6. Vegetation phenological metrics obtained by different methods. (a) Liaoning Nanfen iron mining area; (b) Inner Mongolia Sanheming iron mining area; (c) Sichuan Hongge iron mining area.

vegetation phenology was determined. The final influence distance was acquired by calculating the maximum average value of the influence distance of the different methods (Fig. 8). In LNMA, the influence distance of mining activities on surrounding vegetation phenology was 1566.95 m, which directly caused a delay in SOS by 1.1 ± 0.4 days and a shortening of LOS by 1.0 ± 0.6 days. The influence distance of mining activities on the phenology of surrounding vegetation in IMMA was 1959.67 m, which directly caused SOS to be delayed by 6.1 ± 1.9 days and LOS to be shortened by 5.4 ± 2.5 days. The influence distance of mining activities on the phenology of surrounding vegetation in SCMA was 1809.61 m, which directly caused SOS to be delayed by 1.5 ± 0.7 days, EOS to be advanced by 3.6 ± 1.8 days, and LOS to be shortened by 5.1 ± 3.9 days. In general, the mining activities of LNMA and IMMA had the greatest effect on the SOS of the surrounding vegetation, while the mining activities of SCMA had a greater effect on LOS than SOS and EOS.

4.3. Spatial distribution of affected vegetation

By analyzing the exponential changes in the surrounding phenological metrics of mining areas, it was observed that mining activity has a slight impact on the phenology outside the influence distance and the most significant effect on SOS (LNMA and IMMA) and LOS (SCMA). Therefore, the mean SOS (or LOS) outside the influence distance was used as the threshold to classify the SOS (or LOS) within the influence distance to quantify the spatial distribution of the impact of mining activities on the surrounding vegetation. The affected vegetation obtained by different smoothing methods had a highly similar spatial distribution and area (Table 1, Fig. 9). For different mining areas, within the influence distance, SCMA had the largest proportion of affected vegetation, which was 69.08%, followed by IMMA at 63.74%, and LNMA had the smallest proportion of 59.08%. These affected vegetation were mainly distributed around mining intensive areas and large stopes.

It was also important to recognize the response of vegetation phenology to mining activities by dividing the intensity and scale of mining activities. To this end, mining activities in the study areas were divided into intensive areas (② and ⑥ in Fig. 9), scattered areas (①, ③, ⑤, and ⑦), and single large mines (④ and Fig. 9b) based on field surveys and remote sensing survey data. Intensive area was the main area that affected vegetation phenology. Its affected area was 59.30 km^2, accounting for 46.44% of the vegetation in the affected area. The area of affected vegetation in scattered areas was 31.72 km^2, accounting for 24.84%. Moreover, the area of affected vegetation in the single large stope was 36.67 km^2, accounting for 28.72%.

5. Discussion

5.1. The impact of mining activities on vegetation phenology

The results showed that no matter the scale of mining area large or small, the closer to the mining activity area, the greater the difference in phenology. We provided further insights into how the mining activities affect the changes in the surrounding vegetation phenology. Specifically, the impact of the main environmental problems caused by mining activities on vegetation phenology was analyzed based on remote sensing, field surveys, and existing research. The survey found that 1) the decreases in groundwater level were mainly caused by the deep excavation of stopes, 2) the tailings pond was the main source of waterborne pollution, and 3) a large amount of dust pollution was caused by other mining activities, such asore transportation and waste rock accumulation. Fig. 10a shows that intensive areas and large stopes are the main areas affecting vegetation, suggesting that the environmental impact of mining is related to the intensity and scale of mining activities (Edwards et al., 2014). The factors influencing vegetation phenology varied from area to area. For the intensive areas which consisted of many mining and concentration industries, the main factors included the dust pollution, the decrease in groundwater level, and the waterborne pollution (Fig. 10a). For the scattered areas which dominated by concentrated industries, the main factors included the dust pollution and the waterborne pollution caused by mining activities. For the single large stope area, the main factor was the decrease in groundwater level caused by mine drainage. For example, ore transportation in region A produced severe dust pollution; a large amount of dust adhered to the vegetation, causing the SOS of the vegetation in this area to be delayed by about 23 days, EOS was advanced by about 15 days, and the LOS was reduced by about 37 days (Fig. 10b). This is because dust pollution affected respiration, transpiration, and photosynthesis, allowed the penetration of phytotoxic gaseous pollutants, and led to a general decline in the productivity of the vegetation (Farmer,

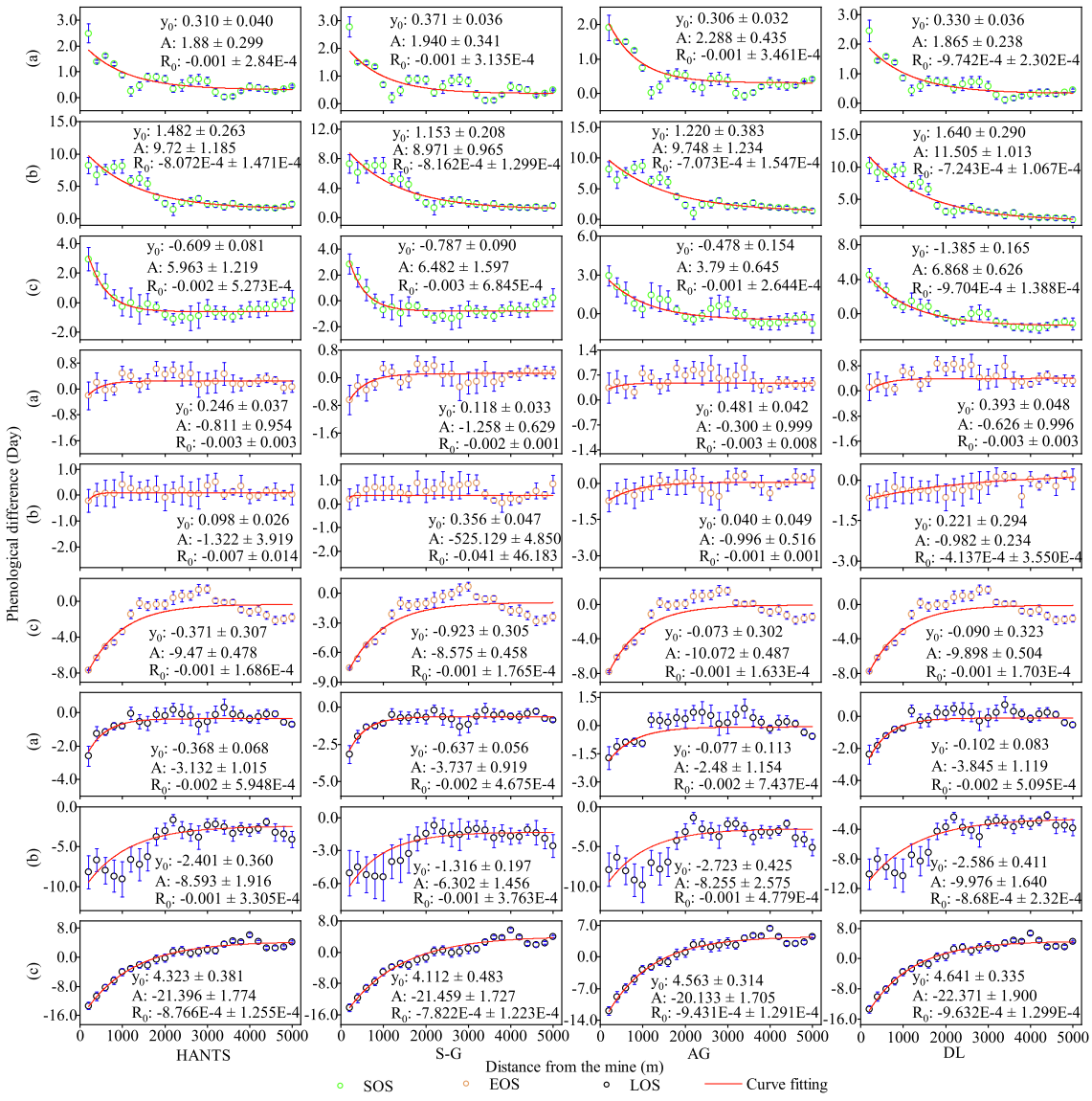

Fig. 7. Changes of phenological metrics in the mining areas. (a) Liaoning Nanfen iron mining area; (b) Inner Mongolia Sanheming iron mining area; (c) Sichuan Hongge iron mining area.

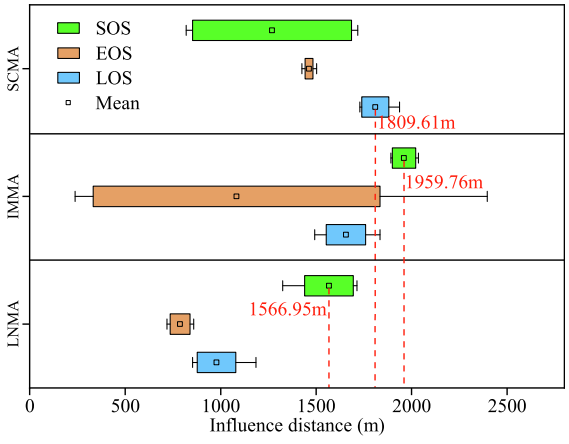

Fig. 8. Influence distance of mining activities in different mining areas on vegetation.

1993; Kameswaran et al., 2019; Watkinson et al., 2021). In region B, with an increase in mining depth, a slope of 552 m that formed locally (Tao et al., 2017) directly affected the underground habitat of vegetation and caused the SOS in this area to be delayed by about five days, EOS was advanced by about one day, and the LOS was reduced by about six days (Fig. 10c). This is because the transpiration of groundwater on plants is very important in the ecosystem, particularly in areas with chronic or transient water shortages (Barbeta and Peñuelas, 2017). During the mining process, the mine drainage caused the groundwater level to decrease, and the groundwater flow system was affected, which led to changes in the vegetation growth and caused vegetation degradation in the areas surrounding those where mining activities were taking place (Maihemuti et al., 2021; Sun et al., 2021). In region C, mining activities produced a large amount of acidic drainage containing heavy metals, which negatively affected the environment and caused the SOS in this area to be delayed by about 19 days, EOS was advanced by about 14 days, and the LOS was reduced by about 33 days (Fig. 10d). This is because these wastewaters were toxic to most organisms and limited the acclimation of vegetation and natural succession in mining areas (Pająk et al., 2018). Overall, dust pollution, groundwater level drop, and waterborne pollution were the main factors that directly

Table 1
Area of affected vegetation surrounding mining activities. (Area: km^2).

Model	HANTS		S-G		AG		DL		Mean	
	Area	Percentage	Area	Percentage	Area	Percentage	Area	Percentage	Area	Percentage
LNMA	43.49	55.29%	46.81	59.50%	49.06	62.36%	46.55	59.17%	46.48	59.08%
IMMA	22.07	63.59%	22.13	63.74%	22.40	64.53%	21.90	63.08%	22.12	63.74%
SCMA	59.13	69.13%	59.38	69.43%	58.54	68.44%	59.30	69.33%	59.09	69.08%
Intensive area	58.38	46.82%	60.19	46.91%	59.22	45.56%	59.39	46.49%	59.30	46.44%
Scattered area	30.21	24.23%	31.84	24.81%	32.66	25.12%	32.18	25.19%	31.72	24.84%
Single large mine	36.10	28.95%	36.28	28.28%	38.11	29.32%	36.18	28.32%	36.67	28.72%

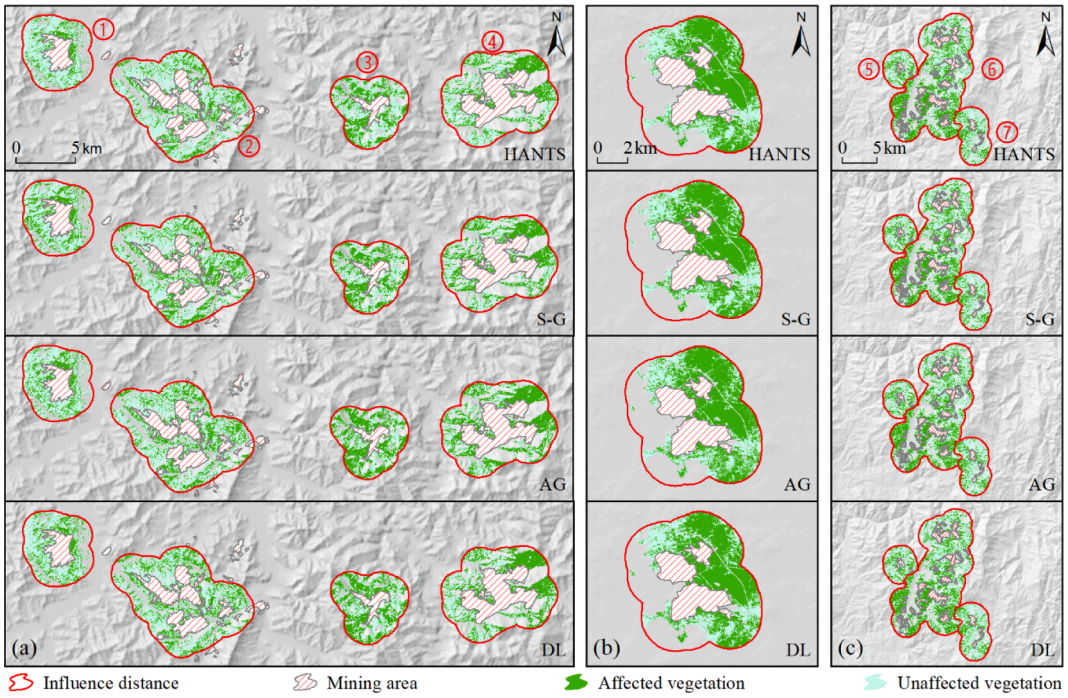

Fig. 9. Spatial distribution of affected vegetation surrounding mining activities. (a) Liaoning Nanfen iron mining area; (b) Inner Mongolia Sanheming iron mining area; (c) Sichuan Hongge iron mining area.

affected the phenological changes around mining areas.

Additionally, Fig. 7 shows that the mining activities of LNMA and IMMA had a greater impact on SOS than EOS, which indicated that the effects of the environmental factors on phenology varied with the site and that SOS was generally more sensitive to environmental factors (White et al., 2002; Wang et al., 2019).

5.2. *Factors controlling the impact of mining activities on vegetation phenology*

Earlier studies have shown that mining and its scale are the main factors affecting the surrounding environment (Johnson and Hallberg, 2005; Sun et al., 2020); that is, the larger the mining scale, the greater the impact on the environment. The results in our study revealed that the mining activity area of each mining area was in the following order: LNMA (40.55 km^2) > SCMA (20.45 km^2) > IMMA (11.98 km^2), but its influence distance on the surrounding vegetation was IMMA (1959.76 m) > SCMA (1809.61 m) > LNMA (1566.95 m). This showed that other factors also controlled the impact of mining activities on the surrounding vegetation phenology in addition to the mining scale. As phenology varied greatly over broad geographic gradients and was controlled by many environmental factors (Richardson et al., 2013), this study adopted the contrast method to analyze the difference in influence distance and degree of mining activities on the surrounding vegetation from two aspects of climate and topography.

For LNMA and SCMA with the same topography, although the mining scale of LNMA was much larger than that of SCMA, the influence distance of LNMA on the surrounding vegetation was 150.15 m less than that of SCMA. The impact degree of LNMA on surrounding phenology was also less than SCMA; that is, the mean of $\triangle SOS_{LNMA}$ was 1.1 days, which was less than 1.5 days of $\triangle SOS_{SCMA}$; the mean of $\triangle LOS_{LNMA}$ was 1.0 day, which was less than 5.1 days of $\triangle LOS_{SCMA}$. Moreover, the proportion of affected vegetation area within the influence distance of SCMA was 10% higher than that of LNMA. Through comparing the evaporation and precipitation in the two regions (Fig. 11), it was found that the drought of the SCMA was much greater than that of the LNMA. Therefore, the drought may be one of the main factors that control the influence distance and degree of mining activities on the surrounding vegetation phenology. This is because vegetation phenology is more sensitive to drought (Luo et al., 2021). Depleting groundwater levels caused by mining activities aggravated water resource problems in arid areas, affecting the growth, distribution, and succession of the surrounding vegetation (Mi et al., 2021). Similar effects of groundwater depletion on vegetation in mining areas have been found in other regions of the world, for example, mining-induced dewatering depletes groundwater storage surrounding mine sites, then causes a drop in the mean vegetation conditions in Europe and Africa by 25% and 1%, respectively (Shen et al., 2021). Similar conclusions were reported in

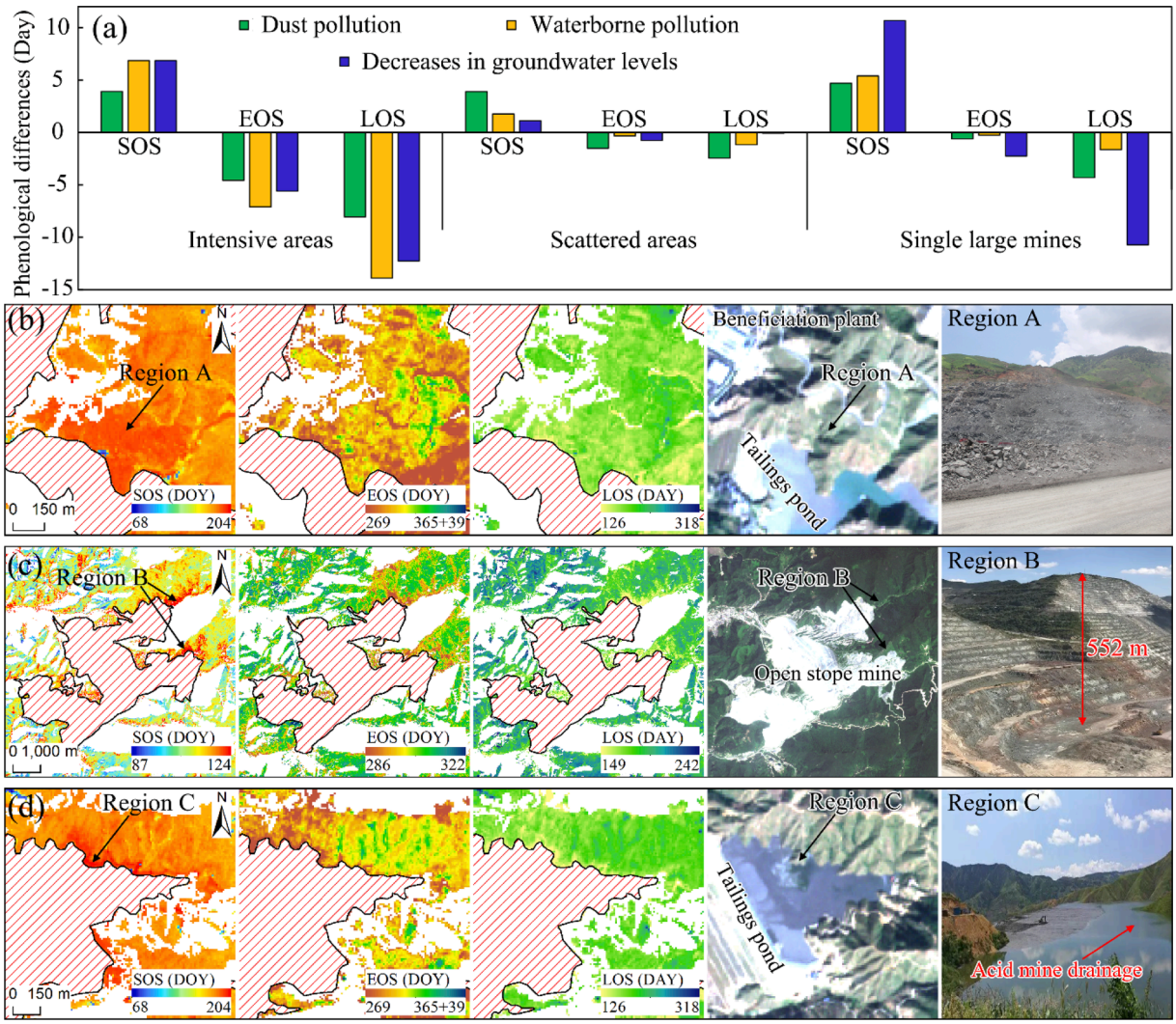

Fig. 10. (a) The impact degree of environmental problems on vegetation phenology in different regions; (b-d) the main factors and site photos of the impact of mining activities on vegetation.

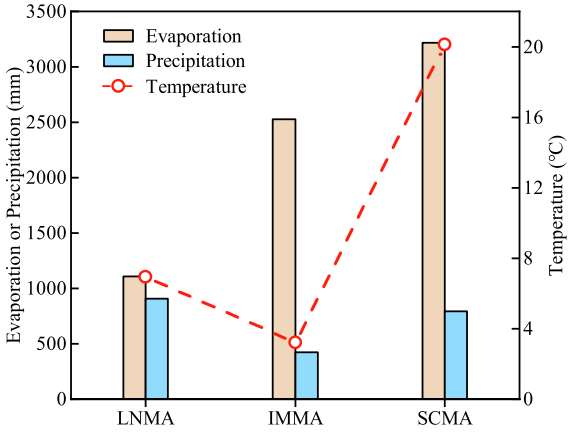

Fig. 11. Precipitation, temperature, and evaporation in the study area.

Nevada by Albano et al. (2020), where almost all water withdrawals for mining came from groundwater and then led to a decline in vegetation vigor around the mining area. In addition, the humid climate in the LNMA mitigated the impact of groundwater depletion caused by mining activities on vegetation phenology to a certain extent (Rishmawi et al., 2016). In conclusion, mining-induced groundwater level changes in arid areas have greater long-term and latent impacts on vegetation than those in humid areas.

For both IMMA and SCMA in arid areas, the influence distance of IMMA on surrounding vegetation was 243.02 m more than that of SCMA, and the impact degree of IMMA was greater than that of SCMA, even though the mining scale of IMMA was much smaller than SCMA. Specifically, the mean of $\triangle SOS_{IMMA}$ was 6.1 days, which was greater than 1.5 days of $\triangle SOS_{SCMA}$; the mean of $\triangle LOS_{IMMA}$ was 5.4 days, which was greater than 5.1 days of $\triangle LOS_{SCMA}$. Comparing the topography of the two regions, it was found that the average relief amplitude of SCMA (62 m) was much greater than that of IMMA (8 m). Therefore, topography may also be a factor that controls the influence distance and degree of mining activities on the surrounding vegetation phenology, and this hypothesis can be mutually confirmed by the correspondence between wind direction and phenology (Fig. 12). Dominated by northwest and southwest winds (163 days), the IMMA had almost 30 days shorter LOS in the northeast and southeast regions than in other directions (Fig. 12b). For the SCMA, the south wind (199 days) prevailed, but the northern LOS was about 15 days shorter than the southwest (Fig. 12c). There are two main reasons for the inconsistent relationship between wind direction and phenology in these two arid regions. One is that the terrain of the SCMA is low in the south (1,335 m) and high in the north (1,750 m), and the high-altitude terrain in the north hinders the

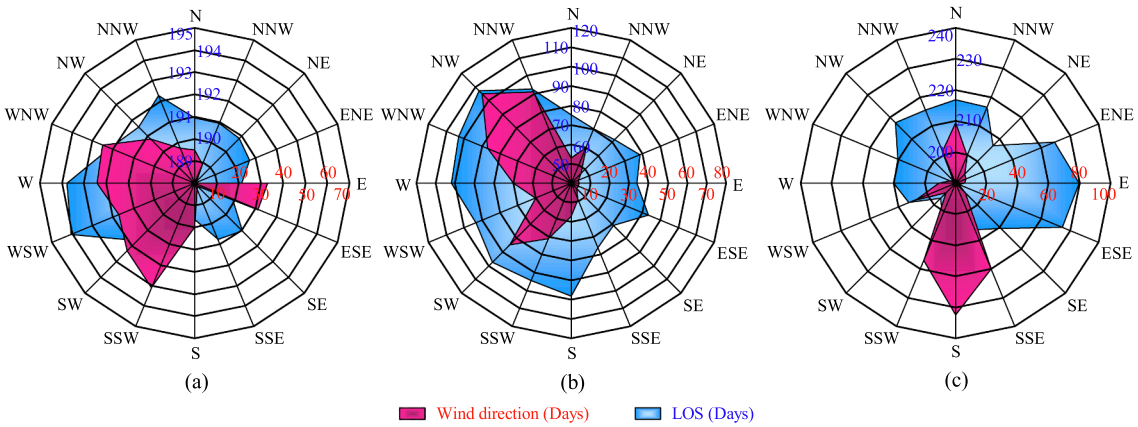

Fig. 12. Correspondence between wind direction and vegetation phenology. (a) Liaoning Nanfen iron mining area; (b) Inner Mongolia Sanheming iron mining area; (c) Sichuan Hongge iron mining area.

spread of dust. The other is that the distribution of mining activities is affected by topography (Chen et al., 2012; Adhikari et al., 2022). In the SCMA, the stopes on the western slope of mountain accout for about 82%, and the mining activities (e.g., ore transportation, concentration industry and dumping ground) distributed along the southwest direction accout for about 71%. Similarly, the LOS in the northeast direction of the LNMA that dominated by the southwest wind, was slightly lower than in the southwest (Fig. 12a).

Our study showed that the distance and degree of the impact of mining activities on phenology were closely related to drought and topography. This conclusion is supported by the existing research results. As shown in ecosystem carbon gain studies, under severe drought conditions in areas dominated by herbs and shrubs, vegetation greening is delayed, shrub senescence is accelerated, and phenological differences between herbs and shrubs will lead to a reduction in potential ecosystem carbon gain (Esch et al., 2019). Recent studies have also demonstrated that warming (or mining)-induced drought could limit carbon sequestration by reducing the rate of cell production, and a longer LOS will not benefit the growth of vegetation located in drought areas (Gao et al., 2022). In addition, pollution dispersion studies have shown that topography mainly affects the formation and dispersion of pollutants through local humidity, airflow and temperature patterns, and boundary layers, especially in areas with complex topography such as mountains, valleys, and basins (Wang et al., 2019). Common types of pollution, like land pollution, water pollution, and air pollution are influenced by topography (Haldane & Kneese, 2019). Numerous studies have shown that global warming has greatly altered vegetation phenology (Keenan et al., 2014). However, a comparison of the three mining areas showed that temperature might not be a factor that controls the influence distance and degree of mining activities on the surrounding vegetation phenology. On the one hand, there was no obvious change in the temperature around the mining area during the mining process. On the other hand, the mean of the phenology index outside the buffer zone was used as the reference phenology, and the difference between the phenological metrics in the buffer zone and the reference phenology were compared, which eliminated the impact of climate change.

6. Conclusion

In our study, a method was proposed to quantify the impact of mining activities on vegetation based on the Sentinel-2 time series and Pareto principle, and was applied to the LNMA, the IMMA, and the SCMA in China. The influence distances of mining activities on vegetation were 1566.95 m, 1959.67 m, and 1809.61 m for the LNMA, the IMMA, and the SCMA respectively. In terms of the influence level, SOS was delayed by 1.1 ± 0.4 days, 6.1 ± 1.9 days and 1.5 ± 0.7 days in the LNMA, the IMMA and the SCMA, respectively, while LOS was shortened by 1.0 ± 0.6 days, 5.4 ± 2.5 days and 5.1 ± 3.9 days in the LNMA, the IMMA and the SCMA, respectively. The SCMA had the largest proportion 69.08% of the affected area (59.09 km^2) of vegetation to total vegetation area within the influence distance, followed by the IMMA with a proportion of 63.74% (22.12 km^2) and the LNMA with a proportion of 59.08% (46.48 km^2). Intensive areas and single large stopes were the main mining activity areas that affected vegetation, and the areas of affected vegetation around these areas were 59.30 km^2 and 36.67 km^2, respectively. The affected vegetation area in the scattered area was 31.72 km^2, accounting for only 24.84% of the total affected vegetation area. The impact of mining activities on vegetation was not only related to the scale of mining but was also closely related to the degree of drought and topography of the mining area. The more arid the area, the more fragile the ecological environment, and the greater the impact of mining activities on vegetation. Topography controlled the distribution of mining activities and the resulting environmental pollution of mining area. Additionally, dust pollution, the drop of groundwater level, and waterborne pollution were the main factors that directly affecting the phenological changes around mining areas.

These results suggest that in addition to the mining activity areas, the surrounding areas should also be considered in environmental monitoring, management, and restoration of mine. These findings can provide data support and help to related departments for conducting mine management in a more targeted manner and optimizing the mine environment restoration plan. Given the limited availability of Sentinel-2 images, only three representative iron mining areas are selected for analysis in this study. Future studies can adopt the method developed in this study to investigate more mining areas to verify the utility of the method.

Declaration of Competing Interest

The authors declare that they have no known competing financial interests or personal relationships that could have appeared to influence the work reported in this paper.

Acknowledgments

This study was supported and funded by the National Natural Science Foundation of China (Grant No. 42074021; Grant No. 42001310), the Department of Science and Technology of Sichuan Province (Grant No. 2020YFS0530; Grant No. 2020JDTD0003), the Science and Technology Bureau of Nanchong City (Grant Nos. 21YFZJ0034), and the China Scholarship Council (CSC No. 202007000081).

References

Adhikari, S., Marcelo-Silva, J., Rajakaruna, N., Siebert, S.J., 2022. Influence of land use and topography on distribution and bioaccumulation of potentially toxic metals in soil and plant leaves: A case study from Sekhukhuneland, South Africa. Sci. Total Environ. 806, 150659. https://doi.org/10.1016/j.scitotenv.2021.150659.

Adole, T., Dash, J., Atkinson, P.M., 2018. Characterising the land surface phenology of Africa using 500 m MODIS EVI. Appl. Geogr. 90, 187–199. https://doi.org/10.1016/j.apgeog.2017.12.006.

Albano, C.M., McGwire, K.C., Hausner, M.B., McEvoy, D.J., Morton, C.G., Huntington, J. L., 2020. Drought sensitivity and trends of riparian vegetation vigor in Nevada, USA (1985–2018). Remote Sensing 12 (9), 1362. https://doi.org/10.3390/rs12091362.

Atkinson, P.M., Jeganathan, C., Dash, J., Atzberger, C., 2012. Inter-comparison of four models for smoothing satellite sensor time-series data to estimate vegetation phenology. Remote Sens. Environ. 123, 400–417. https://doi.org/10.1016/j.rse.2012.04.001.

Baetens, L., Desjardins, C., Hagolle, O., 2019. Validation of copernicus Sentinel-2 cloud masks obtained from MAJA, Sen2Cor, and FMask processors using reference cloud masks generated with a supervised active learning procedure. Remote Sensing 11 (4), 433. https://doi.org/10.3390/rs11040433.

Barbeta, A., Peñuelas, J., 2017. Relative contribution of groundwater to plant transpiration estimated with stable isotopes. Sci. Rep. 7 (1), 1–10. https://doi.org/10.1038/s41598-017-09643-x.

Beck, P.S., Atzberger, C., Høgda, K.A., Johansen, B., Skidmore, A.K., 2006. Improved monitoring of vegetation dynamics at very high latitudes: A new method using MODIS NDVI. Remote Sens. Environ. 100 (3), 321–334. https://doi.org/10.1016/j.rse.2005.10.021.

Bolton, D.K., Gray, J.M., Melaas, E.K., Moon, M., Eklundh, L., Friedl, M.A., 2020. Continental-scale land surface phenology from harmonized Landsat 8 and Sentinel-2 imagery. Remote Sens. Environ. 240, 111685. https://doi.org/10.1016/j.rse.2020.111685.

Buyantuyev, A., Wu, J., 2012. Urbanization diversifies land surface phenology in arid environments: interactions among vegetation, climatic variation, and land use pattern in the Phoenix metropolitan region, USA. Landscape Urban Plann. 105 (1–2), 149–159. https://doi.org/10.1016/j.landurbplan.2011.12.013.

Castellazzi, P., Longuevergne, L., Martel, R., Rivera, A., Brouard, C., Chaussard, E., 2018. Quantitative mapping of groundwater depletion at the water management scale using a combined GRACE/InSAR approach. Remote Sens. Environ. 205, 408–418. https://doi.org/10.1016/j.rse.2017.11.025.

Chaussard, E., Kerosky, S., 2016. Characterization of black sand mining activities and their environmental impacts in the Philippines using remote sensing. Remote Sensing 8 (2), 100. https://doi.org/10.3390/rs8020100.

Chen, J., Jönsson, P., Tamura, M., Gu, Z., Matsushita, B., Eklundh, L., 2004. A simple method for reconstructing a high-quality NDVI time-series data set based on the Savitzky-Golay filter. Remote Sens. Environ. 91 (3–4), 332–344. https://doi.org/10.1016/j.rse.2004.03.014.

Chen, Y., Liu, Y., Liu, Y., Lin, A., Kong, X., Liu, D., Li, X., Zhang, Y., Gao, Y., Wang, D., 2012. Mapping of Cu and Pb contaminations in soil using combined geochemistry, topography, and remote sensing: A case study in the Le'an River floodplain, China. Int. J. Environ. Res. Public Health 9 (5), 1874–1886. https://doi.org/10.3390/ijerph9051874.

Dai, X., Gao, Y., He, X., Liu, T., Jiang, B., Shao, H., Yao, Y., 2021. Spatial-temporal pattern evolution and driving force analysis of ecological environment vulnerability in Panzhihua City. Environ. Sci. Pollut. Res. 28 (6), 7151–7166. https://doi.org/10.1007/s11356-020-11013-6.

Edwards, D.P., Sloan, S., Weng, L., Dirks, P., Sayer, J., Laurance, W.F., 2014. Mining and the African environment. Conservation Letters 7 (3), 302–311. https://doi.org/10.1111/conl.12076.

Efron, B., 1986. Double exponential families and their use in generalized linear regression. J. Am. Stat. Assoc. 81 (395), 709–721.

Esch, E.H., Lipson, D.A., Cleland, E.E., 2019. Invasion and drought alter phenological sensitivity and synergistically lower ecosystem production. Ecology 100 (10), e02802. https://doi.org/10.1002/ecy.2802.

Espada, R., 2018. Return period and Pareto analyses of 45 years of tropical cyclone data (1970–2014) in the Philippines. Appl. Geogr. 97, 228–247. https://doi.org/10.1016/j.apgeog.2018.04.018.

Farmer, A.M., 1993. The effects of dust on vegetation—a review. Environ. Pollut. 79 (1), 63–75. https://doi.org/10.1016/0269-7491(93)90179-R.

Firozjaei, M.K., Sedighi, A., Firozjaei, H.K., Kiavarz, M., Homaee, M., Arsanjani, J.J., Makki, M., Naimi, B., Alavipanah, S.K., 2021. A historical and future impact assessment of mining activities on surface biophysical characteristics change: A remote sensing-based approach. Ecol. Ind. 122, 107264. https://doi.org/10.1016/j.ecolind.2020.107264.

Forkuor, G., Ullmann, T., Griesbeck, M., 2020. Mapping and monitoring small-scale mining activities in Ghana using sentinel-1 time series (2015–2019). Remote Sensing 12 (6), 911. https://doi.org/10.3390/rs12060911.

Gallwey, J., Robiati, C., Coggan, J., Vogt, D., Eyre, M., 2020. A Sentinel-2 based multispectral convolutional neural network for detecting artisanal small-scale mining in Ghana: Applying deep learning to shallow mining. Remote Sens. Environ. 248, 111970. https://doi.org/10.1016/j.rse.2020.111970.

Gao, S., Liang, E., Liu, R., Babst, F., Camarero, J.J., Fu, Y.H., Piao, S., Rossi, S., Shen, M., Wang, T., Peñuelas, J., 2022. An earlier start of the thermal growing season enhances tree growth in cold humid areas but not in dry areas. Nat. Ecol. Evol. 6 (4), 397–404. https://doi.org/10.1038/s41559-022-01668-4.

Gao, X., Gray, J.M., Reich, B.J., 2021. Long-term, medium spatial resolution annual land surface phenology with a Bayesian hierarchical model. Remote Sens. Environ. 261, 112484. https://doi.org/10.1016/j.rse.2021.112484.

Haldane, JBS., Kneese, AV. (2015). Quality of the environment: an economic approach to some problems in using land, water and air. London, UK: Routledge. https://doi.org/10.4324/9781315676937.

He, F., Gu, L., Wang, T., Zhang, Z., 2017. The synthetic geo-ecological environmental evaluation of a coastal coal-mining city using spatiotemporal big data: a case study in Longkou, China. J. Cleaner Prod. 142, 854–866. https://doi.org/10.1016/j.jclepro.2016.07.011.

Hird, J.N., McDermid, G.J., 2009. Noise reduction of NDVI time series: An empirical comparison of selected techniques. Remote Sens. Environ. 113 (1), 248–258. https://doi.org/10.1016/j.rse.2008.09.003.

Hmimina, G., Dufrêne, E., Pontailler, J.-Y., Delpierre, N., Aubinet, M., Caquet, B., de Grandcourt, A., Burban, B., Flechard, C., Granier, A., Gross, P., Heinesch, B., Longdoz, B., Moureaux, C., Ourcival, J.-M., Rambal, S., Saint André, L., Soudani, K., 2013. Evaluation of the potential of MODIS satellite data to predict vegetation phenology in different biomes: An investigation using ground-based NDVI measurements. Remote Sens. Environ. 132, 145–158. https://doi.org/10.1016/j.rse.2013.01.010.

Ivits, E., Cherlet, M., Tóth, G., Sommer, S., Mehl, W., Vogt, J., Micale, F., 2012. Combining satellite derived phenology with climate data for climate change impact assessment. Global Planet. Change 88, 85–97. https://doi.org/10.1016/j.gloplacha.2012.03.010.

Johnson, D.B., Hallberg, K.B., 2005. Acid mine drainage remediation options: a review. Sci. Total Environ. 338 (1–2), 3–14. https://doi.org/10.1016/j.scitotenv.2004.09.002.

Jönsson, P., Eklundh, L., 2002. Seasonality extraction by function fitting to time-series of satellite sensor data. IEEE Trans. Geosci. Remote Sens. 40 (8), 1824–1832. https://doi.org/10.1109/TGRS.2002.802519.

Jönsson, P., Eklundh, L., 2004. TIMESAT—a program for analyzing time-series of satellite sensor data. Comput. Geosci. 30 (8), 833–845. https://doi.org/10.1016/j.cageo.2004.05.006.

Li, X., Zhou, Y., Meng, L., Asrar, G.R., Lu, C., Wu, Q., 2019. A dataset of 30 m annual vegetation phenology indicators (1985–2015) in urban areas of the conterminous United States. Earth Syst. Sci. Data 11 (2), 881–894. https://doi.org/10.5194/essd-11-881-2019.

Litvinenko, V.S., 2020. Digital economy as a factor in the technological development of the mineral sector. Nat. Resour. Res. 29 (3), 1521–1541. https://doi.org/10.1007/s11053-019-09568-4.

Luo, M., Meng, F., Sa, C., Duan, Y., Bao, Y., Liu, T., De Maeyer, P., 2021. Response of vegetation phenology to soil moisture dynamics in the Mongolian Plateau. CATENA 206, 105505. https://doi.org/10.1016/j.catena.2021.105505.

Maihemuti, B., Simayi, Z., Alifujiang, Y., Aishan, T., Abliz, A., Aierken, G., 2021. Development and evaluation of the soil water balance model in an inland arid delta oasis: Implications for sustainable groundwater resource management. Global Ecol. Conserv. 25, e01408. https://doi.org/10.1016/j.gecco.2020.e01408.

Main-Knorn, M., Pflug, B., Louis, J., & Debaecker, V. (2015). Calibration and validation plan for the L2A processor and products of the Sentinel-2 mission. In Proceedings of International Symposium on Remote Sensing of Environment (ISRSE) 2015 (Vol. 40, No. W3, pp. 1249-1255). Copernicus Publications. DOI: 10.5194/isprsarchives-XL-7-W3-1249-2015.

Maryati, S., Shimada, H., Hamanaka, A., Sasaoka, T., Matsui, K., 2012. Determine appropriate post mining land use in Indonesia coal mining using land suitability evaluation. Journal of Novel Carbon Resource Sciences 5, 33–38.

McDonald, P., Mayes, R., Pini, B., 2012. Mining work, family and community: A spatially-oriented approach to the impact of the Ravensthorpe nickel mine closure in remote Australia. Journal of Industrial Relations 54 (1), 22–40. https://doi.org/10.1177/0022185611432382.

Melaas, E.K., Sulla-Menashe, D., Gray, J.M., Black, T.A., Morin, T.H., Richardson, A.D., Friedl, M.A., 2016. Multisite analysis of land surface phenology in North American temperate and boreal deciduous forests from Landsat. Remote Sens. Environ. 186, 452–464. https://doi.org/10.1016/j.rse.2016.09.014.

Mi, J.X., Liu, R., Zhang, S.L., Hou, H., Yang, Y., Chen, F., Zhang, L., 2019. Vegetation patterns on a landslide after five years of natural restoration in the Loess Plateau mining area in China. Ecol. Eng. 136, 46–54. https://doi.org/10.1016/j.ecoleng.2019.05.022.

Mi, J., Yang, Y., Hou, H., Zhang, S., Raval, S., Chen, Z., Hua, Y., 2021. The long-term effects of underground mining on the growth of tree, shrub, and herb communities in arid and semiarid areas in China. Land Degrad. Dev. 32 (3), 1412–1425. https://doi.org/10.1002/ldr.3751.

Misra, G., Cawkwell, F., Wingler, A., 2020. Status of phenological research using Sentinel-2 data: A review. Remote Sensing 12 (17), 2760. https://doi.org/10.3390/rs12172760.

Norris, J.R., Walker, J.J., 2020. Solar and sensor geometry, not vegetation response, drive satellite NDVI phenology in widespread ecosystems of the western United States. Remote Sens. Environ. 249, 112013. https://doi.org/10.1016/j.rse.2020.112013.

Kameswaran, S., Gunavathi, Y., Krishna, P.G., 2019. Dust pollution and its influence on vegetation-a critical analysis. Research Journal of Life Sciences, Bioinformatics, Pharmaceutical and Chemical Sciences 5 (1), 341–363.

Kandasamy, S., Fernandes, R., 2015. An approach for evaluating the impact of gaps and measurement errors on satellite land surface phenology algorithms: Application to 20 year NOAA AVHRR data over Canada. Remote Sens. Environ. 164, 114–129. https://doi.org/10.1016/j.rse.2015.04.014.

Keenan, T.F., Gray, J., Friedl, M.A., Toomey, M., Bohrer, G., Hollinger, D.Y., Munger, J. W., O'Keefe, J., Schmid, H.P., Wing, I.S., Yang, B., Richardson, A.D., 2014. Net carbon uptake has increased through warming-induced changes in temperate forest phenology. Nat. Clim. Change 4 (7), 598–604. https://doi.org/10.1038/nclimate2253.

Odell, S.D., Bebbington, A., Frey, K.E., 2018. Mining and climate change: A review and framework for analysis. The extractive industries and society 5 (1), 201–214. https://doi.org/10.1016/j.exis.2017.12.004.

Padhee, S.K., Dutta, S., 2019. Spatio-temporal reconstruction of MODIS NDVI by regional land surface phenology and harmonic analysis of time-series. GIScience & Remote Sensing 56 (8), 1261–1288. https://doi.org/10.1080/15481603.2019.1646977.

Pająk, M., Błońska, E., Szostak, M., Gąsiorek, M., Pietrzykowski, M., Urban, O., Derbis, P., 2018. Restoration of vegetation in relation to soil properties of spoil heap heavily contaminated with heavy metals. Water Air Soil Pollut. 229 (12), 1–15. https://doi.org/10.1007/s11270-018-4040-6.

Parmesan, C., Yohe, G., 2003. A globally coherent fingerprint of climate change impacts across natural systems. Nature 421 (6918), 37–42. https://doi.org/10.1038/nature01286.

Press, W., Teukolsky, A., Vetterling, W., Flannery, B., 1992. Numerical Recipes in C, Second edition. Cambridge University Press, New York.

Qiu, S., Zhu, Z., He, B., 2019. Fmask 4.0: Improved cloud and cloud shadow detection in Landsats 4–8 and Sentinel-2 imagery. Remote Sens. Environ. 231, 111205. https://doi.org/10.1016/j.rse.2019.05.024.

Richardson, A.D., Keenan, T.F., Migliavacca, M., Ryu, Y., Sonnentag, O., Toomey, M., 2013. Climate change, phenology, and phenological control of vegetation feedbacks to the climate system. Agric. For. Meteorol. 169, 156–173. https://doi.org/10.1016/j.agrformet.2012.09.012.

Rishmawi, K., Prince, S.D., Xue, Y., 2016. Vegetation responses to climate variability in the northern arid to sub-humid zones of Sub-Saharan Africa. Remote Sensing 8 (11), 910. https://doi.org/10.3390/rs8110910.

Rohith, G., & Kumar, L. S. (2020, July). Remote sensing signature classification of agriculture detection using deep convolution network models. In International Conference on Machine Learning, Image Processing, Network Security and Data Sciences (pp. 343-355). Springer, Singapore. https://doi.org/10.1007/978-981-15-6315-7_28.

Rudke, A.P., Sikora de Souza, V.A., Santos, A.M.D., Freitas Xavier, A.C., Rotunno Filho, O.C., Martins, J.A., 2020. Impact of mining activities on areas of environmental protection in the southwest of the Amazon: a GIS-and remote sensing-based assessment. J. Environ. Manage. 263, 110392. https://doi.org/10.1016/j.jenvman.2020.110392.

Shao, H., Sun, X., Lin, Y., Xian, W., Zhou, Y., Yuan, L., Qi, J., 2021. A method for spatio-temporal process assessment of eco-geological environmental security in mining areas using catastrophe theory and projection pursuit model. Progress in Physical Geography: Earth and Environment 45 (5), 647–668. https://doi.org/10.1177/0309133320982542.

Shen, Z., Zhang, Q., Piao, S., Peñuelas, J., Stenseth, N.C., Chen, D., Xu, C.-Y., Singh, V.P., Liu, T., 2021. Mining can exacerbate global degradation of dryland. Geophys. Res. Lett. 48 (21) https://doi.org/10.1029/2021GL094490.

Sola, I., García-Martín, A., Sandonís-Pozo, L., Álvarez-Mozos, J., Pérez-Cabello, F., González-Audícana, M., Llovería, R.M., 2018. Assessment of atmospheric correction methods for Sentinel-2 images in Mediterranean landscapes. Int. J. Appl. Earth Obs. Geoinf. 73, 63–76. https://doi.org/10.1016/j.jag.2018.05.020.

Sonderegger, T., Berger, M., Alvarenga, R., Bach, V., Cimprich, A., Dewulf, J.o., Frischknecht, R., Guinée, J., Helbig, C., Huppertz, T., Jolliet, O., Motoshita, M., Northey, S., Rugani, B., Schrijvers, D., Schulze, R., Sonnemann, G., Valero, A., Weidema, B.P., Young, S.B., 2020. Mineral resources in life cycle impact assessment—part I: a critical review of existing methods. The International Journal of Life Cycle Assessment 25 (4), 784–797. https://doi.org/10.1007/s11367-020-01736-6.

Sun, X., Shao, H., Xiang, X., Yuan, L., Zhou, Y., Xian, W., 2020. A coupling method for eco-geological environmental safety assessment in mining areas using PCA and catastrophe theory. Nat. Resour. Res. 29 (6), 4133–4148. https://doi.org/10.1007/s11053-020-09682-8.

Sun, X., Zhou, Y., Yuan, L., Li, X., Shao, H., Lu, X., 2021. Integrated decision-making model for groundwater potential evaluation in mining areas using the cusp catastrophe model and principal component analysis. J. Hydrol.: Reg. Stud. 37, 100891. https://doi.org/10.1016/j.ejrh.2021.100891.

Tao, Z.G., Meng, X.Z., Ma, C.R., Zhu, C., He, M.C., Wang, C.J., Zhang, H.J., 2017. Analysis of wedge-shaped landslide mechanism and sliding force monitoring warning in Nanfen open pit iron mine. J. China Coal Soc 42, 3149–3158.

Thanh Noi, P., Kappas, M., 2018. Comparison of random forest, k-nearest neighbor, and support vector machine classifiers for land cover classification using Sentinel-2 imagery. Sensors 18 (1), 18. https://doi.org/10.3390/s18010018.

Tost, M., Hitch, M., Chandurkar, V., Moser, P., Feiel, S., 2018. The state of environmental sustainability considerations in mining. J. Cleaner Prod. 182, 969–977. https://doi.org/10.1016/j.jclepro.2018.02.051.

Verbesselt, J., Hyndman, R., Newnham, G., Culvenor, D., 2010. Detecting trend and seasonal changes in satellite image time series. Remote Sens. Environ. 114 (1), 106–115. https://doi.org/10.1016/j.rse.2009.08.014.

Wang, X.C., Klemeš, J.J., Dong, X., Fan, W., Xu, Z., Wang, Y., Varbanov, P.S., 2019a. Air pollution terrain nexus: A review considering energy generation and consumption. Renew. Sustain. Energy Rev. 105, 71–85. https://doi.org/10.1016/j.rser.2019.01.049.

Wang, X., Xiao, J., Li, X., Cheng, G., Ma, M., Zhu, G., Altaf Arain, M., Andrew Black, T., Jassal, R.S., 2019b. No trends in spring and autumn phenology during the global warming hiatus. Nat. Commun. 10 (1) https://doi.org/10.1038/s41467-019-10235-8.

Watkinson, A.D., Virgl, J., Miller, V.S., Naeth, M.A., Kim, J., Serben, K., Shapka, C., Sinclair, S., 2021. Effects of dust deposition from diamond mining on subarctic plant communities and barren-ground caribou forage. Effects of dust deposition from diamond mining on sub-arctic plant communities and barren-ground caribou forage. 50 (4), 990–1003. https://doi.org/10.1002/jeq2.20251.

White, M.A., Nemani, R.R., Thornton, P.E., Running, S.W., 2002. Satellite evidence of phenological differences between urbanized and rural areas of the eastern United States deciduous broadleaf forest. Ecosystems 5 (3), 260–273. https://doi.org/10.1007/s10021-001-0070-8.

Wu, Z., Lei, S., Lu, Q., Bian, Z., Ge, S., 2020. Spatial distribution of the impact of surface mining on the landscape ecological health of semi-arid grasslands. Ecol. Ind. 111, 105996. https://doi.org/10.1016/j.ecolind.2019.105996.

Xin, Q., Li, J., Li, Z., Li, Y., Zhou, X., 2020. Evaluations and comparisons of rule-based and machine-learning-based methods to retrieve satellite-based vegetation phenology using MODIS and USA National Phenology Network data. Int. J. Appl. Earth Obs. Geoinf. 93, 102189. https://doi.org/10.1016/j.jag.2020.102189.

Yu, L.e., Xu, Y., Xue, Y., Li, X., Cheng, Y., Liu, X., Porwal, A., Holden, E.-J., Yang, J., Gong, P., 2018. Monitoring surface mining belts using multiple remote sensing datasets: A global perspective. Ore Geol. Rev. 101, 675–687. https://doi.org/10.1016/j.oregeorev.2018.08.019.

Zhang, J., Zhao, J., Wang, Y., Zhang, H., Zhang, Z., Guo, X., 2020. Comparison of land surface phenology in the Northern Hemisphere based on AVHRR GIMMS3g and MODIS datasets. ISPRS J. Photogramm. Remote Sens. 169, 1–16. https://doi.org/10.1016/j.isprsjprs.2020.08.020.

Zhang, X., Goldberg, M.D., 2011. Monitoring fall foliage coloration dynamics using time-series satellite data. Remote Sens. Environ. 115 (2), 382–391. https://doi.org/10.1016/j.rse.2010.09.009.

Zhang, X., Tarpley, D., Sullivan, J.T., 2007. Diverse responses of vegetation phenology to a warming climate. Geophys. Res. Lett. 34 (19) https://doi.org/10.1029/2007GL031447.

Zhou, D., Zhao, S., Zhang, L., Liu, S., 2016. Remotely sensed assessment of urbanization effects on vegetation phenology in China's 32 major cities. Remote Sens. Environ. 176, 272–281. https://doi.org/10.1016/j.rse.2016.02.010.

Zhou, D., Zhao, S., Zhang, L., Sun, G., Liu, Y., 2015. The footprint of urban heat island effect in China. Sci. Rep. 5, 11160. https://doi.org/10.1038/srep11160.